Progress in Oceanography 127 (2014) 108–116

Contents lists available at ScienceDirect

Progress in Oceanography

journal homepage: www.elsevier.com/locate/pocean

How much do tides affect the circulation of the Mediterranean Sea? From local processes in the Strait of Gibraltar to basin-scale effects

C. Naranjo [a,*], J. Garcia-Lafuente [a], G. Sannino [b], J.C. Sanchez-Garrido [a]

[a] Physical Oceanography Group, University of Málaga, CEIMAR, Málaga, Spain
[b] ENEA, Ocean Modelling Unit, via Anguillarese 301, 00123 Rome, Italy

ARTICLE INFO

Article history:
Received 20 December 2013
Received in revised form 23 June 2014
Accepted 23 June 2014
Available online 1 July 2014

ABSTRACT

The effects of tidal forcing on the exchange flow through the Strait of Gibraltar and the circulation in the near-field region are revisited with a regional numerical model. Also a basin-scale model run is conducted in a first attempt to assess the impact of these local processes on the Western Mediterranean thermohaline circulation. In the Strait of Gibraltar, tides are found to (1) increase the exchange flow volume transport, (2) modify the hydrological properties of Atlantic inflowing waters through the enhancement of mixing, and (3) facilitate the drainage of Mediterranean deep water. In the far-field, the model reveals that these local processes can favor deep convection in the Gulf of Lion. Some thoughts are provided offering possible explanations.

Introduction

The baroclinic exchange through the Strait of Gibraltar (SoG hereinafter) is forced by the buoyancy losses in the Mediterranean Sea (MS). They give rise to the characteristic anti-estuarine thermohaline circulation of the MS that starts at the SoG with the surface Atlantic Jet and ends at the same location with the deep outflow of Mediterranean waters. The average properties of the latter are basically determined by the buoyancy losses and the constraining topography of the SoG (Fig. 1), which drives the intervening flows to the hydraulic limit and to a situation of maximal exchange (Armi and Farmer, 1985, 1986; Farmer and Armi, 1988). Within this theoretical frame, Bryden and Kinder (1991) resolved the steady, two-layer maximal exchange problem for a simple but yet realistic geometry of the SoG by imposing the mean net evaporation over the MS as the proper reservoir condition. Despite ignoring some of the relevant driving forces, the approach gives realistic predictions of the exchange.

The exchange involves different time-scales (Garcia-Lafuente et al., 2000, 2002a, 2002b) and the forces ignored in the previous models, essentially tidal forces and meteorologically-driven pressure gradients should be included to obtain more accurate predictions. Theoretical (Farmer and Armi, 1986; Helfrich, 1995), laboratory (Helfrich, 1995), numerical (Wang, 1993; Sannino et al., 2004) and observational (Bryden et al., 1994; Vargas et al., 2006) studies show that tides increase the long-term exchange flow by means of eddy-fluxes. The easiest way to visualize this process is by decomposing the velocity and the layer thickness in slowly varying (overbar) and fluctuating (primed) components according to $u = \bar{u} + u', h = \bar{h} + h'$ (in practice, the decomposition is achieved by applying a suitable filter). The slow-varying flow, often called long-term flow, is defined as the exchange resulting from the time-average of the flow over a time window considerably longer than the tidal scale and is obtained as

$$\bar{q}_l = W\left(\bar{u}_l\bar{h}_l + \overline{u_l'h_l'}\right) \tag{1}$$

The first term of the right hand side is the quasi-steady contribution due to the mean fields whereas the second term is the eddy fluxes. Here W is a representative width and $i = 1, 2$ indicates the Atlantic and Mediterranean layers. According to the observational analysis by Bryden et al. (1994), eddy-fluxes may account for up to 40% of the estimated long term flow. Subsequent experimental studies show that they depend on the location of the cross-section where they are computed (Garcia-Lafuente et al., 2000; Baschek et al., 2001; Sanchez-Román et al., 2009), a result also reported in the numerical study by Sannino et al. (2004). Eddy fluxes show a clear dependence on the fortnightly tidal cycle (Vargas et al., 2006). The total flow, however, is less sensitive to the fortnightly tide since the enhanced mixing driven by strong currents during spring tides diminishes the quasi steady term in (1) and counterbalances the increased eddy-flux (Bryden et al., 1994; Vargas

* Corresponding author. Address: Grupo Oceanografía Física, ETSI Telecomunicación, Universidad de Málaga, Campus de Teatinos s/n, 29071 Málaga, Spain. Tel.: +34 952132849.

E-mail address: cnaranjo@ctima.uma.es (C. Naranjo).

http://dx.doi.org/10.1016/j.pocean.2014.06.005
0079-6611/

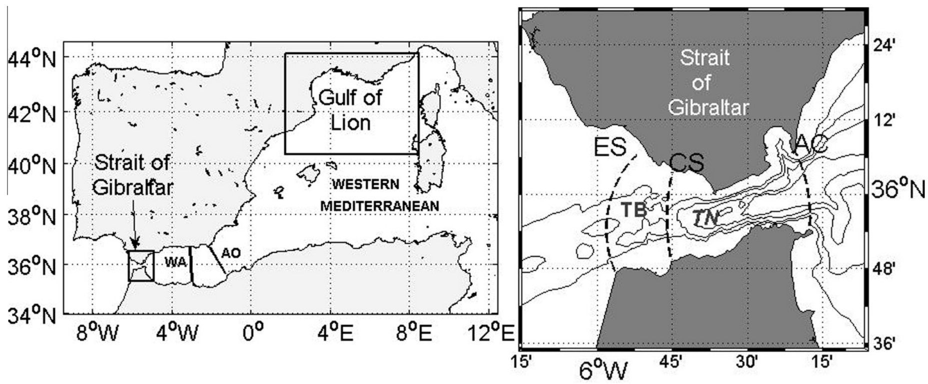

Fig. 1. Left panel shows the Western Mediterranean Sea. The upper rectangle indicates the control volume in the Gulf of Lion used to compute the results of Section 'Basin scale processes, WMDW formation'. WA in the Alborán Basin indicates the Western Alborán section mentioned in the text, and AO indicates the Almería-Orán front. The lower small rectangle encloses the Strait of Gibraltar (SoG), which is zoomed on in the right panel. In this panel, ES, CS and AC indicate Espartel Sill, Camarinal Sill and Algeciras–Ceuta sections, respectively, which are used for doing computations. TN represents Tarifa Narrows and TB is the Tangier Basin that extends from CS to ES. Isobaths every 200 m are shown from the surface to 1000 m.

et al., 2006). This result agrees with the findings of Helfrich (1995) who shows that the exchange increases with the frequency and the strength of the barotropic fluctuations.

While the effect of tides on the volume transport is relatively well known, other processes are not. Tidally-induced mixing in the Camarinal sill area (CS hereinafter, Fig. 1) is remarkably pronounced across the internal hydraulic jump at the western flank of the sill, and grows particularly vigorously when the shear between Atlantic and Mediterranean layer is enhanced by tidal flows. This leads to flow instability and turbulence as revealed by the observation of Kelvin–Helmholtz billows and energy dissipation rates as large as 10^{-2} W kg^{-1} (Wesson and Gregg, 1994), which are among the greatest ever recorded in the ocean. Sanchez-Garrido et al. (2011) show that the flow instabilities keep occurring in additional hydraulic transitions downstream of smaller-scale topographic features located in the Tangier Basin (Fig. 1), which enlarges the mixing area to the west. As a result, this basin is a remarkable source of Atlantic–Mediterranean mixed water that can be advected in either direction (Garcia-Lafuente et al., 2013). Furthermore, tides are the origin of propagating internal bores and large amplitude nonlinear internal waves (Farmer and Armi, 1988; Vázquez et al., 2008; Sanchez-Garrido et al., 2013) with clear potential to increase mixing elsewhere in the SoG (Garcia-Lafuente et al., 2013). Whatever the specific process involved, mixing is so strong that it invalidates the simple description of the exchange in terms of two layers and requires the inclusion of a third interface mixing layer, which participates actively in the dynamic of the exchange (Bray et al., 1995; Sannino et al., 2007).

The physical and biological consequences of this mixing in the nearby Alborán Sea basin and further east in the MS are poorly addressed and are awaiting for more in depth studies. According to several authors (Macías et al., 2007, 2008; Vázquez et al., 2009; Garcia-Lafuente et al., 2011, 2013) and as mentioned previously, a considerable volume of the biologically enriched waters in the area of strong mixing in CS is advected eastward, and eventually helps fertilize the Alborán Sea. In his paleoclimate study of the MS, Mikolajewicz (2011) found that the numerically modeled sea surface temperature in the Alborán Sea was greater than the observed climatology. He attributed this mismatch to the absence of tidal forcing in his model, which reduces the vertical turbulent fluxes of heat and salt. The result is a slightly warmer and more buoyant inflowing Atlantic surface water when tides are not included. The effect might be far-reaching taking into account that this inflow will be finally transformed into intermediate and/or deep Mediterranean water.

Another relevant issue for the MS circulation is the renewal of deep Mediterranean waters and the ventilation of the bottom layer. Western Mediterranean Deep Water (WMDW), which is formed in the Northwestern MS and spreads later over the Western Mediterranean basin, resides well below the main sill of Camarinal and must be uplifted above the sill depth in order to leave the MS. The required energy would be supplied by the spatial acceleration that the flow undergoes as it approaches the SoG (Bernoulli suction), a topic which has been addressed in different studies (Stommel et al., 1973; Bryden and Stommel, 1982; Whitehead, 1985; Garcia-Lafuente et al., 2007, 2009; Naranjo et al., 2012). The remarkable intensity of tidal currents in the SoG is a relevant energy source for the aspiration of deep water that has not been mentioned in the literature except for the paper by Kinder and Bryden (1990). These authors detected traces of WMDW in the ocean side of the sill at the end of the west-going phase of some tidal cycles in spring tides, and speculated about the possibility that WMDW were routinely uplifted by tides. The authors left the issue open for further research.

The present work addresses these topics with the help of two numerical models that have been run with and without tidal forcing in order to compare their outputs and thus assess the influence of tides on several hydrodynamic relevant features. The work is organized as follows. Section 'Numerical models' describes the most relevant aspects of the numerical models already used in previous studies, which the readers are referred to for details. Section 'Tides increase the long-term exchange flows' revisits the relevant issue of the tidally-forced eddy fluxes in the SoG in the light of the new results provided by the models. Section 'Tides modify the hydrological properties of inflowing water' addresses the changes that tidally-induced mixing cause in the Atlantic inflow in the Alborán Sea and further east. Section 'Tides favor Mediterranean deep water ventilation through the SoG' analyses the influence that tides could possibly have on the ventilation of WMDW near the SoG due to an enhanced Bernoulli suction. All these topics are of rather local or regional nature. In contrast, Section 'Basin scale processes, WMDW formation' addresses the far-field influence of tides by analyzing hindcast events of WMDW formation during the decade of 1960. Section 'Discussion and conclusion' summarizes the findings and conclusions of the study.

Numerical models

The results of two numerical models based on the Massachusetts Institute of Technology general circulation model (MITgcm; Marshall et al., 1997a, 1997b) have been used in this study.

The first model (RSGM, hereinafter) is sub-basin scale and it is described in detail by Sanchez-Garrido et al. (2013). Just a brief summary is given here. The model uses the free-surface and hydrostatic configuration of the MITgcm and its domain covers the Gulf of Cádiz and the Alborán Sea. It is horizontally discretized with a curvilinear grid of variable spatial resolution. In order to better reproduce the mixing processes and the vorticity field in the SoG, the maximum resolution is achieved in the strait with a horizontal mesh size of around 300–500 m for both Δx and Δy, which gradually increases to some kilometers toward the east and west open boundaries. In the vertical the model has 46 unevenly distributed z-levels, with minimum cell thickness at the surface ($\Delta z = 5$ m). Vertical eddy viscosity and diffusivity coefficients are calculated according to the parameterization of Pacanowski and Philander (1981), whereas the turbulence closure scheme by Leith (1968) is chosen for the horizontal viscosity. The model is driven at the lateral open boundaries by the tracer and velocity fields provided by the Mediterranean forecast model (Oddo et al., 2009), whereas tides are introduced by forcing the model laterally with the tidal velocities produced by the barotropic tidal model of Carrère and Lyard (2003). The model was run for a two-year spin-up period after which it produces realistic outputs.

The second model (GMSM, hereinafter) covers the whole MS, a brief overview is given here. Its grid is non-uniform, curvilinear orthogonal as well, with maximum horizontal resolution of about $1/200° \times 1/200°$ (456 m) in the SoG. Eastwards and westwards of the SoG the resolution diminishes progressively until it reaches a grid size of $1/16° \times 1/16°$ (5.7 km) in the rest of the domain. To resolve the dynamics of the different water masses in the MS adequately, 73 unevenly spaced vertical z-levels were used, whose thickness range from 3 m at the surface to 300 m at the ocean bottom. The model is forced at the surface by the wind stress and the heat and fresh water fluxes derived from the dynamical downscaling of ECMWF ERA40 reanalysis performed with the regional atmospheric model RegCM (Artale et al., 2009). A surface relaxation to climatological temperature (5 days) and salinity (30 days) are also applied. Tides are incorporated in the model and tidal forcing includes both the tide generating potential as a body force in the momentum equations, and the lateral boundary condition in the open Atlantic boundary, which is imposed in the same way as in the RSGM model.

Both models have been run with and without tidal forcing in order to assess the local, regional and far-reaching effects of the tides. The characteristics of RSGM model make it more suitable for addressing local and regional issues as it produces hourly values compared to daily-means in GMSM; its outputs are used throughout Sections 'Tides increase the long-term exchange flows' and 'Tides modify the hydrological properties of inflowing water'. Although the simulation run covered the years 2010–2011, only the period from September to December 2011 has been used in this study. The period has been intentionally chosen because it coincides with the period analyzed in Sanchez-Garrido et al. (2013) and Sammartino et al. (2014), during which a comprehensive model validation was carried out. The GMSM model is used to address the question of how tides in the SoG could possibly affect relevant physical processes in the MS far away from the very strait, namely the deep water formation processes in the Gulf of Lion. This study makes use of the 1958–1968 hindcast in Sections 'Tides favor Mediterranean deep water ventilation through the SoG' and 'Basin scale processes, WMDW formation'.

Tides increase the long-term exchange flows

This section revisits the issue of how tide-induced eddy-fluxes increase the exchanged flows, with the help of the RGSM model, which has proven to be more accurate than the one presented by Sannino et al. (2004) (see model comparison in Sannino et al., 2014). Following Garcia-Lafuente et al. (2000) and Baschek et al. (2001) the volume transport through a given cross-section is calculated by taking as the interface between Atlantic and Mediterranean waters the isohaline that maximizes the transport. A fresher isohaline would ascribe eastward-flowing Atlantic water to the Mediterranean layer, thus diminishing both the estimated inflow and the outflow. The same would occur if a saltier isohaline were selected, since westward-flowing Mediterranean water would be ascribed to the Atlantic layer. Fig. 2 shows that this isohaline can always be found, although its specific value changes with the location. It also changes in the tidal and non-tidal runs at the same location. Table 1 shows the computed volume transport at CS section and at the two boundaries of the SoG, namely Espartel (ES, see Fig. 1) and Algeciras–Ceuta (AC) sections, along with the isohaline that maximizes the exchange in both runs.

Focusing on section CS, the maximum exchange is achieved for isohalines 37.3 and 37.1 for the tidal and non-tidal runs, respectively, and the corresponding transports are 0.84 Sv and 0.79 Sv, respectively, 6% higher in the tidal run. At ES, the isohaline that maximizes the flow is 36.6 (Fig. 2, Table 1) in both runs, an expected lower salinity than at CS. The transport at ES in the two experiments is larger than at CS, with the tidal run still giving a $\sim$6% greater value (0.98 Sv versus 0.93 Sv). The lower salinity of the isohaline used as interface and the larger flow at ES compared with CS section are attributable to the entrainment of AW by the swift Mediterranean undercurrent in the western part of the SoG (Garcia-Lafuente et al., 2011). Likewise, the entrainment of MW by the overlying Atlantic jet leads to a more saline interface (around 37.4) and greater flows through AC section than at CS. The tidal run keeps on providing greater transports than the non-tidal run also in this section (0.89 Sv against 0.82 Sv, $\sim$8% increase).

It is interesting and illustrative to explore the decomposition of transport in terms of the slowly-varying and eddy-fluxes contributions (Eq. (1)). Table 1 indicates that the contribution of eddy-fluxes to the total flow at CS is very large (0.32 Sv or 38%), whereas they decrease dramatically to 3% and 1.4% at the bounding sections of ES and AC respectively. These results agree with the findings of Bryden et al. (1994) who reported eddy-fluxes as high as 50% at CS, and with Vargas et al. (2006) who estimated eddy-fluxes of 0.3–0.4 Sv from observations at the same section. The very small eddy fluxes at the ending sections of AC and ES (Table 1) are also in agreement with Garcia-Lafuente et al. (2000) and Baschek et al. (2001) who found eddy-fluxes reduced to less than 5% in a cross section nearby AC, and with Sanchez-Román et al. (2009) who estimated similar percentages at ES. The reason why eddy fluxes are so significant at CS and almost negligible at the ending sections of the strait is related to the internal hydraulics of the SoG. As shown in Sannino et al. (2007) and Sanchez-Garrido et al. (2011) the hydraulic control at CS is not as permanent as at ES or at Tarifa Narrows (Farmer and Armi, 1988), and it is when the hydraulic control at CS is lost that eddy-fluxes participate actively in the mean transport. As long as the hydraulic controls at ES and Tarifa Narrows are not flooded, eddy-fluxes at AC and ES may be neglected (Vargas et al., 2006; Sannino et al., 2007; Sanchez-Garrido et al., 2011).

Another result worth noting in Table 1 is that the exchanged flows in the non-tidal run do not coincide with the slowly-varying contribution of the flows in the tidal run (compare columns 4 and 6 in Table 1). Thus, the result of including tides is not the mere addition of an eddy-flux contribution to the flows computed in the non-tidal run, because this sum does not match the flows in the tidal run. At ES and AC, the quasi-steady part of the flows in the tidal run is already greater than the flows in the non-tidal run, but at CS, however, it is much lower. All this highlights the complexity that tides bring to the actual exchange.

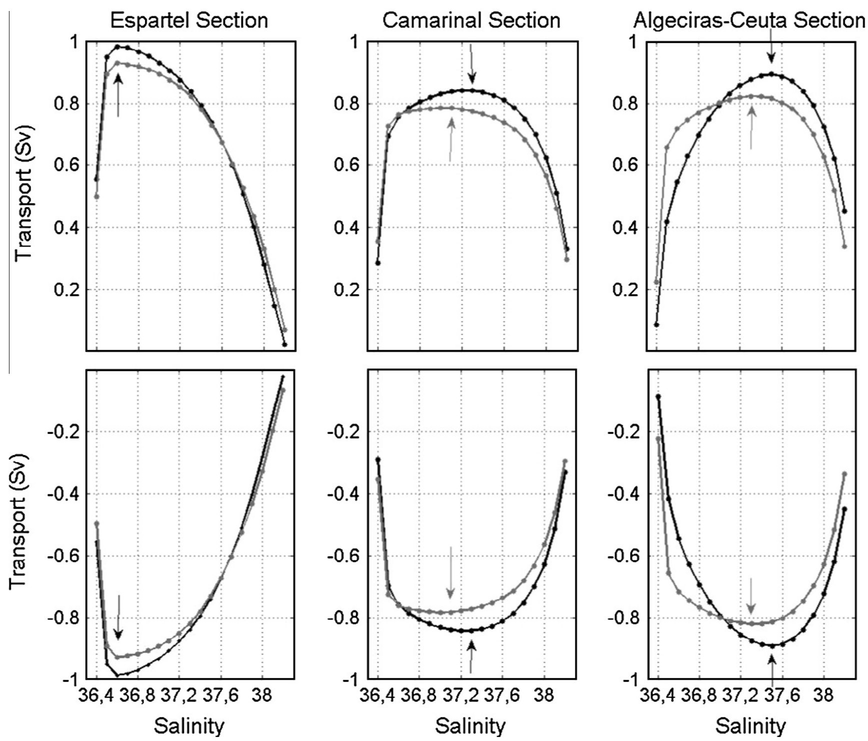

Fig. 2. Atlantic and Mediterranean transports versus the salinity of the isohaline used to calculate it. Black and gray lines correspond to tidal and no-tidal runs, respectively. Arrows indicate the maximum transport with the same color code. Only one arrow is seen at ES because the isohaline that maximizes the transport is the same in both runs.

Table 1
Computed transports (in Sv) at ES, CS and AC sections (see Fig. 1). The first two columns indicate the isohalines that maximizes the transports in each section (see Fig. 2). The third and fourth columns are the mean transport in the tidal and non-tidal runs, respectively, and the fifth column gives the increment (percentage) that tides cause on the transports. The term ($\bar{u}_i\bar{h}_i$), which is representative of the slow-varying term in Eq. (1), is shown in the sixth column. Eddy-fluxes ($\overline{u_i'h_i'}$) and the percentage of the total flow that they account for are shown in the last two columns.

	S_{Tid}	$S_{\mathrm{No\text{-}Tid}}$	$\overline{Q}_{\mathrm{Tid}}$	$\overline{Q}_{\mathrm{No\text{-}Tid}}$	Δ (%)	$\bar{u}_i\bar{h}_i$	$\overline{u_i'h_i'}$	% $\overline{u_i'h_i'}$
ES	36.6	36.6	0.988	0.935	5.7	0.957	0.031	3.0
CS	37.3	37.1	0.844	0.793	6.4	0.522	0.322	38
AC	37.5	37.3	0.893	0.823	8.5	0.880	0.013	1.4

Tides modify the hydrological properties of inflowing water

The most apparent local effect of tides in the SoG is the enhanced mixing driven by shear instabilities and turbulence, whose most noticeable results are the thickening of the interfacial layer and the modification of the hydrological properties of their water. Both issues are addressed in this section using the RGSM model under tidal and non-tidal runs.

The upper panels of Fig. 3 show the interfacial layer thickness produced by each run, calculated by fitting a hyperbolic tangent function to the vertical salinity profiles, following Sannino et al. (2007). Lower panels indicate the depth of the middle interface, which coincides with the inflection point of the fitted hyperbolic tangent function. The panels show that the interfacial layer is shallower in the tidal run and, consequently, covers a greater horizontal extension. Despite this increment, west of CS the thickness of the interfacial layer is much the same in both runs, but the layer becomes markedly thicker (up to 90 m in certain regions) eastwards of CS in the tidal run (Fig. 3a and b). As analyzed in Garcia-Lafuente et al. (2013), the reason for this pattern is the eastward advection of the waters that had been mixed in the Tangier basin during the previous rising tide and in the subsequent release and eastward progression of the internal hydraulic jump formed leeward of CS, which provides energy for maintaining high rates of mixing. The shoaling of the interface is primarily noticeable in north-eastern part of the Strait, where the depth of the middle interface changes from 70 m in non-tidal run to near the surface in the tidal one. The joint effect of the shoaling and thickening of the interface in the eastern half of the SoG in the tidal run is to carry water from below to the surface layers in a more effective way than in the non-tidal run. In other words, AWs are expected to be saltier and colder under tidal forcing and, hence, denser and less buoyant.

These AWs are directly advected into the adjacent Alborán Sea basin so that the tidal run gives colder temperatures not only within the dimensions of the SoG but also beyond its limits. Fig. 4 shows the surface temperature difference between the tidal and non-tidal simulations. The greatest differences are found in the eastern exit of the SoG and along the expected path of the Atlantic Jet in the western Alborán Sea, which confirms that in the tidal run the Jet carries colder water because of the enhanced tidal mixing in the SoG. Even when reduced, this difference is still detectable in the area of the Almería-Orán front at the eastern end of the Alborán basin and along the path of the Algerian current further east. These visual results are confirmed by computing the mean temperature of the incoming AWs across AC section: the inflow is 0.37 °C colder in the tidal run (15.42 °C versus 15.79 °C) and also 0.47 units saltier (36.63 versus 36.16). The joint effect is an inflow 0.45 kg m^{-3} denser in the case of the tidal run and, consequently, the flux of advected buoyancy into the Alborán Sea diminishes. For instance, the advected buoyancy within the 100 upper meters of the water column, computed at the AC section, is 1.13 times lower in the tidal run (2.505 ms^{-2} versus 2.235 ms^{-2}), which may have far-field significant consequences, as the cold and salty signature generated in the SoG is exported by the Algerian current to the interior of the MS.

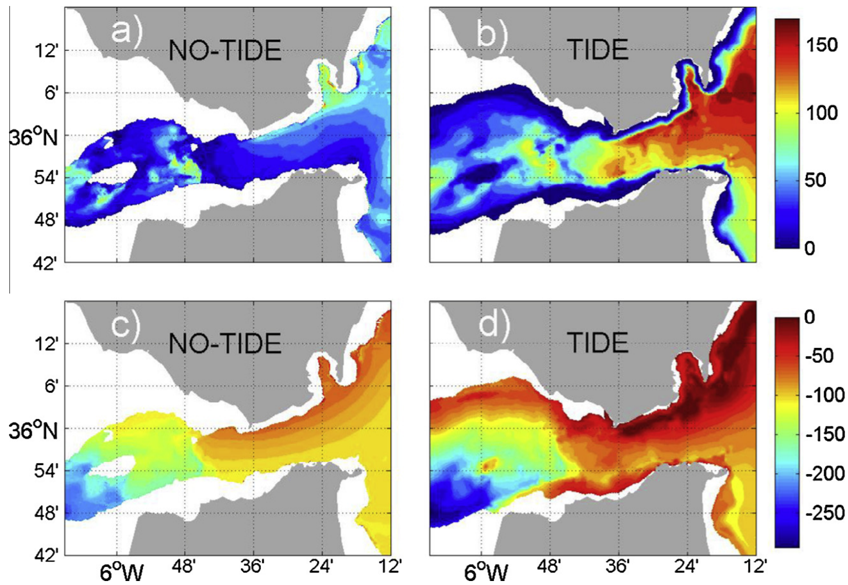

Fig. 3. (a) Interface thickness, in meters, for the non-tidal run. (b) Same as (a) for the tidal run. (c) Mean depth of the interface, in meters, for the non-tidal run. (d) Same as (c) for the tidal run. See text for details about the way they are computed.

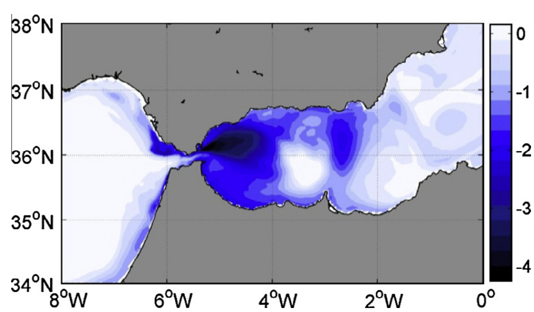

Fig. 4. Surface temperature difference ($\theta_{\text{tides}} - \theta_{\text{no-tides}}$, in °C) between the tidal and non-tidal run in the Alborán Sea.

Tides favor Mediterranean deep water ventilation through the SoG

The GMSM model outputs are examined in this section to address the influence of tides on the draining of the WMDW toward the Atlantic Ocean through the shallow SoG. Prior to investigating the topic, it is convenient to check the model performance, which can be assessed from Fig. 5. The left panel shows the mean temperature and salinity in the AC section (see Fig. 1) provided by the model, whereas panel b) presents observations collected in a nearby cross section. The hydrological properties of the modeled water masses as well as their spatial distribution match remarkably well the observations, particularly in the lower layer, which supports the use of the GMSM model to accomplish the study of the WMDW drainage.

The influence of tides is assessed by comparing the volume of WMDW flowing across the AC section computed for the tidal and non-tidal runs. In the present study, water colder than 13 °C (potential temperature) in the SoG area is considered as WMDW. This criterion, which has been traditionally assumed in the literature (Bryden and Stommel, 1982; Kinder and Parrilla, 1987; Kinder and Bryden, 1990; Garcia-Lafuente et al., 2007, 2009; Naranjo et al., 2012), is convenient in this case because the isotherm $\theta = 13$ °C is sufficiently far from the bottom in both the model and the observations (see Fig. 5) to ensure that it always lies well outside of the bottom boundary layer. Therefore, the estimated flows of WMDW are not critically dependent on the physics of the bottom boundary layer, which is not as well resolved as the ocean interior in the numerical models. Consequently, this weakness is not a major concern for our results.

Table 2 shows the estimated WMDW flow across AC section using the five last years of the GMSM hindcast. Results for the entire 5-year period along with the values for each single year are presented in Table 2. The 5-year average is 28% (0.051 Sv)

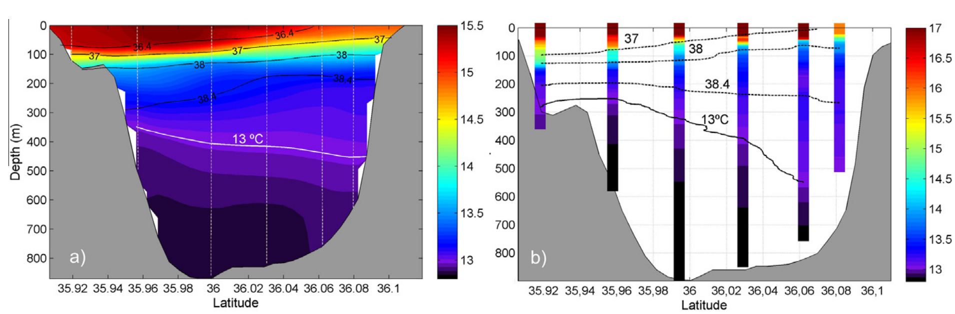

Fig. 5. (a) Mean potential temperature and salinity in section AC (see Fig. 1) derived from the GMSM model outputs. The filled color contours are potential temperature (color bar on the right), while the labeled black contours show the salinity. The white contour is the isotherm $\theta = 13$ °C used as the upper limit of WMDW (see text). (b) CTD profiles collected at the – nearly – same section as in panel (a). The color bar is again for temperature, the dashed black contours are salinity, and the solid black line is the isotherm $\theta = 13$ °C. (For interpretation of the references to color in this figure legend, the reader is referred to the web version of this article.)

Table 2
Time-averaged outflow of water with $\theta < 13$ °C across the AC section (see Fig. 1), which is identified with WMDW in this study. The first row is the five-year average and the remaining rows indicate the year-averaged WMDW outflow. Transport with and without tides are shown in the first two columns. Last column gives the increment between tidal and non-tidal run (ΔQ) and its percentage (%).

Period	Block 1: $\theta < 13$ °C		
	Q_{TID} (Sv)	Q_{NOT} (Sv)	ΔQ (Sv)/%
(1963–1968)	0.233	0.182	0.051/28
1963	0.091	0.060	0.031/51
1964	0.285	0.236	0.049/21
1965	0.307	0.230	0.077/33
1966	0.334	0.303	0.031/10
1967	0.211	0.158	0.052/33

higher in the tidal run, although the percentage fluctuates between 10% and 50% depending on the year. The relevant result regarding this study is the visible enhancement of the WMDW aspiration in the tidal run, but the high year-to-year variability during the simulated period, which we ascribe to the internal variability of the MS and of the WMDW formation processes should also be noted.

A similar procedure has been carried out to estimate the WMDW flow through section WA at 3°W in the Alborán Sea (see Fig. 1). Although the overall estimates point at a slight increase of WMDW volume transport toward the SoG in the tidal run, the analysis is not statistically conclusive. The fact that the comparison of tidal and non-tidal runs does not clearly detect the effect of tides on the WMDW flow through this section, located around 200 km to the east of the SoG, is interpreted as the weakening with the distance of the direct suction by tides.

Basin scale processes, WMDW formation

Deep convection that leads to the formation of WMDW in the northwestern MS is among the most relevant oceanographic processes taking place in this Sea and, as such, it has been extensively discussed in the literature (MEDOC Group, 1969; Schott et al., 1996; Herrmann et al., 2008; Gascard, 1991; Smith et al., 2008; Marshall and Schott, 1999). The convection process involves several phases. The first one is the preconditioning phase (Gascard and Richez, 1985; MEDOC Group, 1969), which comprises the densification processes (buoyancy losses) that the Atlantic surface water undergoes since entering the MS through the SoG until it sinks in winter during the second phase of the convection process. Section 'Tides modify the hydrological properties of inflowing water' of this study has shown that the AW inflow is colder and saltier, i.e., less buoyant, when tides are included in the model and that those signatures are carried eastwards by the Algerian current (Fig. 4). In other words, the AW in the tidal run is more strongly preconditioned than in the non-tidal run.

This section investigates whether or not this difference at the source point (SoG) has a far-field influence on the formation of WMDW in the Gulf of Lion area (Fig. 1). The outputs of the GMSM model run with and without tides are compared to address the issue. Two bulk variables or proxies are analyzed herein: the mixed layer depth (MLD) and the surface area susceptible to participate in the deep convection event (hereinafter DCA). The MLD at each grid point has been defined as the distance from the surface to the depth where the vertical diffusion coefficient reaches a threshold value of 0.04 $m^2\,s^{-1}$, following Herrmann et al. (2008). DCA has been estimated as the area where the surface water is denser than 1029.10 kg m^{-3}, a criterion widely used in the literature of deep convection (Schott et al., 1996; Smith et al., 2008; Pinardi et al., 2013).

Fig. 6 shows the MLD averaged from January to the end of April for every year from 1963 to 1967. Maximum mean MLD reaches 1500 m during 1963, 1964 and 1965, values that are quite similar to those presented by Schott et al. (1996) and Herrmann et al. (2008) in the same area. Except for 1963 MLD in the tidal run is always greater than in the non-tidal run, which is expected if tidal runs better precondition the inflowing AW. Fig. 7 presents the evolution of the estimated DCA during the winter months (January to end of April). The greatest DCA is reached in March 1965 (almost 10×10^{10} m^2 in the tidal run, 2×10^{10} m^2 more than in non-tidal run) followed by 1963; during this year, the DCA is larger in the non-tidal run as was the case for the MLD as well. During the other years, however, the tidal run provides larger DCA than the non-tidal run. A deep water formation rate has been calculated following Lascaratos and Nittis (1998) and is presented in Fig. 8a. Since it combines the former MLD and DCA variables, the comparison of tidal and non-tidal runs does not provide new results but confirms the previous ones, the non-tidal run gives higher formation rates in 1963 and lower rates in all the other years.

The results presented in Figs. 6 and 7 deserve some comentaries despite the topic not being the scope of this work. Focussing on the tidal run, the model simulations predict a great year-to-year variability in all variables, namely MLD, DCA and rate of formation. Notice the reduced DCA in years 1966 and 1967, which is in agreement with the also diminished MLD during these years shown in Fig. 6, which in turn gives the minimum formation rate of barely 0.2 Sv in 1967 (Fig. 8a). On the opposite end is 1965 when the rate of formation approaches 4 Sv, a rather high value that would correspond to an exceptionally productive year. In any case, they fall inside the interval of deep water formation rates reported by other authors that ranges between 0.3 and 6 Sv (Tziperman and Speer, 1994; Krahmann, 1997; Castellari et al., 2000; Herrmann et al., 2008; Béranger et al., 2009; Beuvier et al., 2012; Pinardi

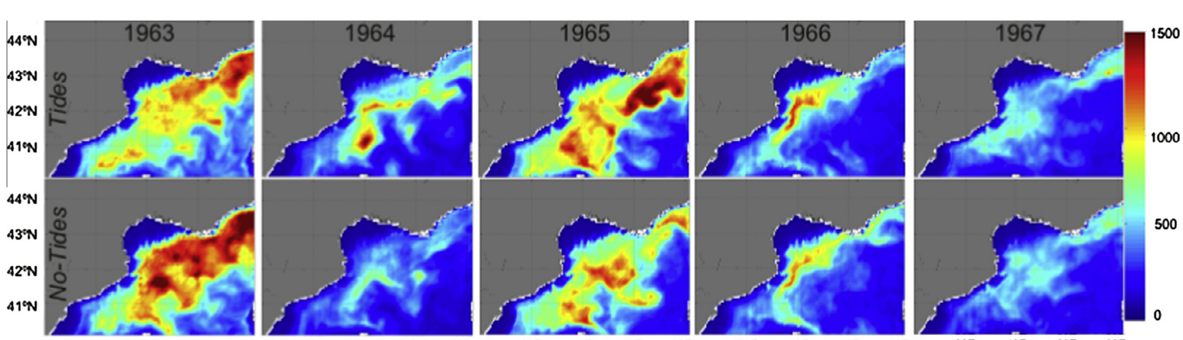

Fig. 6. Mixed layer depth in meters (color bar) in the Gulf of Lion area (see Fig. 1) computed using a threshold value for the vertical diffusion coefficient of 0.04 $m^2\,s^{-2}$. Upper and lower rows correspond to tidal and non-tidal runs, respectively. The contours represent the January-to-April (both included) average. (For interpretation of the references to color in this figure legend, the reader is referred to the web version of this article.)

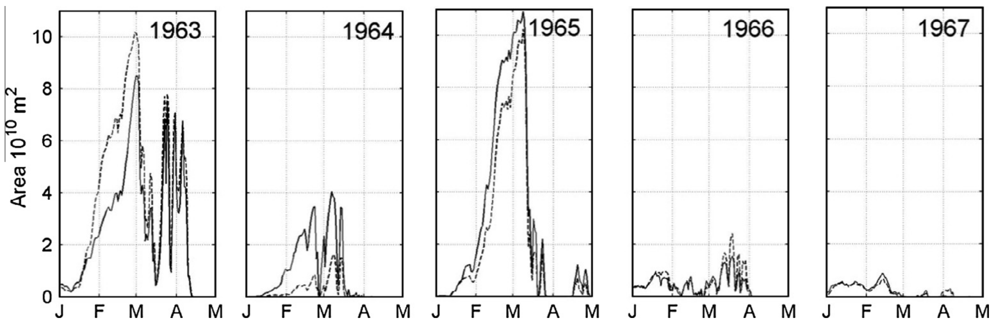

Fig. 7. Time evolution of the Deep Convection Area in the Gulf of Lion (see Fig. 1) from January to the end of April of every year. Solid and dashed lines represent the tidal and non-tidal runs respectively.

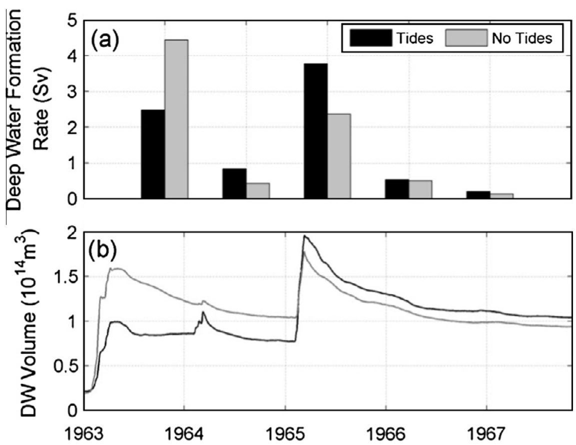

Fig. 8. (a) Deep water formation rate (in Sv) calculated as $(V_A - V_B)/T$, where V_A is the maximum volume in a particular year, V_B is the minimum volume before the convection event and $T = 1$ year $= 3.15 \times 10^7$ s (Lascaratos and Nittis, 1998). (b) Deep water volume measured in the volume control (Fig. 1). Black and gray colors correspond to the tidal and non-tidal run, respectively.

et al., 2013; Schott et al., 1994, 1996; Send et al., 1995; Schroeder et al., 2008; Durrieu de Madron et al., 2013).

Fig. 8b gives the time evolution of the estimated volume of deep water resident in the region of the Gulf of Lion as a function of time. The large formation rate in 1963 filled up the bottom layer, which started draining out once the winter formation processes had finished. The way it did is different for the tidal run, in which the volume decrease stopped after a very short time of drainage and remained constant thereinafter, and the non-tidal run that featured the exponential-like decay expected in this type of physical problem, where the rate of draining must be proportional to the volume of water that is being drained. Notice that, after this year, the drainage after the refilling of the basin predicted in the tidal run shapes an exponential curve reasonably well. We lack of a suitable explanation for the anomalous drainage in 1963, which could be the reason explaining the apparent paradox (according to our hypothesis) of why the non-tidal run predicts a higher rate of formation this year than the tidal run. The footprint of the winter of 1964 is the small cusp, more visible in the tidal run, while 1966 and 1967 with such small rates of deep water formation, hardly leave any signal in the curve. In contrast, 1965 doubled the volume of deep water stored in the Gulf of Lion due to the extraordinary rate of formation, much greater in the tidal run as seen in Fig. 8a.

Discussion and conclusion

This work examines the effect of tides in the SoG on several oceanographic processes whose spatial scales range from local to basin-wide. The most significant outcome is their contribution to increase the mean exchange that is described here, but there are other effects intuitively related to tidal forcing that have not been thoroughly addressed to our knowledge yet. Some of them are investigated in the different sections of this work by comparing the outputs of two numerical models which have been run with and without tidal forcing.

As expected, the model results confirm that the inclusion of tides generate eddy fluxes that increase the long-term exchange. Despite its very similar contribution in the different sections of the SoG (6–8%, see Table 1), the way the increment is achieved differs between sections. At the main CS section, eddy fluxes play a key role and represent a fundamental process to increase the long-term exchange, a result that agrees with previous findings (Bryden et al., 1994; Vargas et al., 2006). At the boundary sections of AC and ES the contribution of eddy fluxes is very small although the increment of the long-term flow due to tides is similar or even higher than at CS (8.5% at AC versus 6.4% at CS, see Table 1). A remarkable result that stems from the weakness of the eddy fluxes at the boundary sections is that the flows could be estimated satisfactorily there using only the slowly-varying term in Eq. (1). It is an interesting outcome for experimental studies because the computation of eddy fluxes from observations poses serious challenges. Actually, some experimental studies (Sanchez-Román et al., 2009; Garcia-Lafuente et al., 2000) have made already use of this flow property.

A second effect of the tides is the enhancement of the mixing between Mediterranean and Atlantic waters within the strait itself. The energy for mixing is mainly released in the various supercritical-to-subcritical flow transitions occurring in the Tangier basin (Sanchez-Garrido et al., 2011). The final outcome is the thickening and shoaling of the interfacial layer in the SoG, which is favored by the propagation of nonlinear internal waves and entrainment of MW by the Atlantic jet, an issue that has been recently addressed by Garcia-Lafuente et al. (2013). These processes are nearly inhibited in the absence of tides, a fact that is reflected by the very thin interfacial mixing layer in the non-tidal simulation (Fig. 3). In addition to the significant effect that the shoaling of the interface may have on biological communities, the tidally-induced mixing also makes the Atlantic jet saltier (0.47 units) and colder (0.37 °C). This water is finally advected to the Alborán Sea which therefore shows colder surface waters almost everywhere, although it is more visible along the mean path of the Atlantic jet and, particularly as it exits the SoG (Fig. 4). As shown recently by Sanchez-Garrido et al. (2013), the 4 °C colder surface water in this area obtained in the tidal simulation has its origin possibly in the advection of positive shear vorticity generated by the interaction of tidal currents with the solid northern boundary of the SoG. If so, this signature would be more related to the local doming of isotherms associated with the enhancement of the cyclonic circulation rather than to the direct advection of colder water from the strait. The downstream temperature anomaly in the Alborán Sea would be a consequence of this process, at least partially, but it does not modify its tidal origin.

Of particular interest is the fact that the cold signature is still clearly visible in the Almería-Orán front and Algerian current, at the eastern exit of the Alborán Sea (dark blue strip over this area in Fig. 4). We hypothesize that the denser AW produced by mixing in the SoG in the tidal run facilitates the formation of WMDW in the Gulf of Lion. The comparison of two bulk variables, namely MLD and DCA, suggests that indeed, the tidal run tends to produce more volume of WMDW. However the first year of the hindcast does not behave so, as the non-tidal run produced more volume of WMDW (Fig. 8).

As mentioned in Section 'Basin scale processes, WMDW formation', we lack an explanation for this behavior, which is further confounded by the fact that this is the only year when the drainage of the WMDW out of the control volume in the tidal run does not follow an expected exponential decay with time (Fig. 7b).

Therefore, the results concerning 1963 must be interpreted with caution. What both models predict in a similar way is the marked year-to-year variability driven by the atmospheric forcing, a variability that has also been found in other studies (Herrmann et al., 2008; Pinardi et al., 2013).

The last issue addressed of whether or not tides favor the ventilation of the deep WMDW layer has a positive answer according to our results. Table 2 indicates that the outflow of WMDW (defined as the water colder than $\theta = 13\,^{\circ}C$ in the neighborhood of the SoG) increases by nearly 30% in the tidal run. This percentage is greater than the 6–7% increment of the long-term outflow due to tides (column 5 in Table 1). The difference in percentages suggests that the drainage of WMDW is specially aided by tides and it is more favored than any of the other Mediterranean waters participating in the outflow. Table 2 also shows an interannual variability that is apparently related to the variability of the WMDW reservoir in the Gulf of Lion revealed in Fig. 8. For instance, the outflow of WMDW reaches its maximum in 1966, a year after the large WMDW formation that occurred in 1965. Taking into account the time the signal will take to travel from the Gulf of Lion to the SoG, this delay seems reasonable (Garcia-Lafuente et al., 2007, 2009). The trend of the WMDW stored in the control volume in the Gulf of Lion is to diminish after 1965 (Fig. 7a), a trend that seems to be followed by the outflow of WMDW with a year delay (Table 2).

In conclusion, our study has provided evidence that tides in the SoG has local (increase of the long-term exchange, noticeable tidally-driven mixing, eventually exported to the MS), regional or short-range (colder and saltier inflow, enhanced aspiration of WMDW) and long-range (influence in deep convection processes) influences. Of all them, the last one is more open to debate because a convincing conclusion requires much longer simulations that include tides in the forcing terms, which are computationally unaffordable at this moment.

Acknowledgments

This work is a contribution to the Spanish funded National Project INGRES 3 (CTM2010-21229) with partially financial support of Project P08-RNM-3738 from Plan Andaluz de Investigación. Cristina Naranjo acknowledges the fellowship BES-2011-043421 from the Ministry of Economy and Competitiveness – Spain. The Mediterranean tidal simulation has been carried out thanks to a CINECA ISCRA grant. The authors are also grateful to the Supercomputing and Bioinformatics (SCBI) Center of the University of Malaga and to CRESCO Supercomputing Facilities at ENEA (www.cresco.enea.it). This is the publication no. 62 from CEIMAR Publication Series.

References

Armi, L., Farmer, D., 1985. The internal hydraulics of the Strait of Gibraltar and associated sills and narrows. Oceanologica Acta 8, 37–46.

Armi, L., Farmer, D.M., 1986. Maximal two-layer exchange through a contraction with barotropic net flow. Journal of Fluid Mechanics 164, 27–51.

Artale, V., Calmanti, S., Carillo, A., Dell'Aquila, A., Herrmann, M., Pisacane, G., Ruti, P.M., Sannino, G., Struglia, M.V., Giorgi, F., Bi, X., Pal, J.S., Rauscher, S., The PROTHEUS Group, 2009. An atmosphere-ocean regional climate model for the Mediterranean area: assessment of a present climate simulation. Climate Dynamics 35, 721–740. http://dx.doi.org/10.1007/s00382-009-0691-8.

Baschek, B., Send, U., Garcia-Lafuente, J., Candela, J., 2001. Transport estimates in the Strait of Gibraltar with a tidal inverse model. Journal of Geophysical Research 106 (C12), 31033–31044. http://dx.doi.org/10.1029/2000JC000458.

Béranger, K., Testor, P., Crépon, M., 2009. Modelling water mass formation in the Gulf of Lion (Mediterranean Sea). In: Briand, F. (Ed.), Dynamics of Mediterranean Deep Waters, CIESM Workshop Monogr, vol. 38. Mediterr. Sci. Comm., Monaco, pp. 91–100.

Beuvier, J., Béranger, K., Lebeaupin-Brossier, C., Somot, S., Sevault, F., Drillet, Y., Bourdallé-Badie, R., Ferry, N., Lyard, F., 2012. Spreading of the Western Mediterranean Deep Water after winter 2005: time scales and deep cyclone transport. Journal of Geophysical Research 117, C07022. http://dx.doi.org/10.1029/2011JC007679.

Bray, N.A., Ochoa, J., Kinder, T.H., 1995. The role of the interface in exchange through the Strait of Gibraltar. Journal of Geophysical Research 100 (C6), 10755–10776. http://dx.doi.org/10.1029/95JC00381.

Bryden, H.L., Kinder, T.H., 1991. Steady two-layer exchange through the Strait of Gibraltar. Deep Sea Research Part A 38, S445–S463. http://dx.doi.org/10.1016/S0198-0149(12)80020-3.

Bryden, H.L., Stommel, H.M., 1982. Origin of the Mediterranean outflow. Journal of Marine Research 40, 55–71.

Bryden, H.L., Candela, J., Kinder, T.H., 1994. Exchange through the Strait of Gibraltar. Progress in Oceanography 33, 201–248. http://dx.doi.org/10.1016/0079-6611(94)90028-0.

Carrère, L., Lyard, F., 2003. Modeling the barotropic response of the global ocean to atmospheric wind and pressure forcing-comparisons with observations. Geophysical Research Letters 30, 1275. http://dx.doi.org/10.1029/2002GL016473.

Castellari, S., Pinardi, N., Leaman, K., 2000. Simulation of the water mass formation processes in the Mediterranean Sea: influence of the time frequency of the atmospheric forcing. Journal of Geophysical Research 105 (C10), 24157–24181. http://dx.doi.org/10.1029/2000JC900055.

Durrieu de Madron, X., Houpert, L., Puig, P., Sanchez-Vidal, A., Testor, P., Bosse, A., Estournel, C., Somot, S., Bourrin, F., Bouin, M.N., Beauverger, M., Beguery, L., Calafat, A., Canals, M., Cassou, C., Coppola, L., Dausse, D., D'Ortenzio, F., Font, J., Heussner, S., Kunesch, S., Lefevre, D., Le Goff, H., Martín, J., Mortier, L., Palanques, A., Raimbault, P., 2013. Interaction of dense shelf water cascading and open-sea convection in the northwestern Mediterranean during winter 2012. Geophysical Research Letters 40, 1379–1385. http://dx.doi.org/10.1002/grl.50331.

Farmer, D.M., Armi, L., 1986. Maximal 2-layer exchange over a sill and through the combination of a sill and contraction with barotropic flow. Journal of Fluid Mechanics 164, 53–76.

Farmer, D.M., Armi, L., 1988. The flow of Mediterranean Water through the Strait of Gibraltar. Progress in Oceanography 21 (1), 1–103.

Garcia-Lafuente, J., Vargas, J.M., Plaza, F., Sarhan, T., Candela, J., Bascheck, B., 2000. Tide at the eastern section of the Strait of Gibraltar. Journal of Geophysical Research 105 (C6), 14197–14213. http://dx.doi.org/10.1029/2000JC900007.

Garcia-Lafuente, J., Delgado, J., Vargas, J.M., Vargas, M., Plaza, F., Sarhan, T., 2002a. Low-frequency variability of the exchanged flows through the Strait of Gibraltar during CANIGO. Deep Sea Research Part II: Topical Studies in Oceanography 49 (19), 4051–4067. http://dx.doi.org/10.1016/S0967-0645(02)00142-X.

Garcia-Lafuente, J., Alvarez Fanjul, E., Vargas, J.M., Ratsimandresy, A.W., 2002b. Subinertial variability in the flow through the Strait of Gibraltar. Journal of Geophysical Research 107 (C10), 3168. http://dx.doi.org/10.1029/2001JC001104.

Garcia-Lafuente, J., Sanchez Roman, A., Díaz del Río, G., Sannino, G., Sanchez-Garrido, J.C., 2007. Recent observations of seasonal variability of the Mediterranean outflow in the Strait of Gibraltar. Journal of Geophysical Research 112, C10005. http://dx.doi.org/10.1029/2006JC003992.

Garcia-Lafuente, J., Delgado, J., Sanchez-Roman, A., Soto, J., Carracedo, L., Díaz-del-Río, G., 2009. Interannual variability of the Mediterranean outflow observed in Espartel sill, western Strait of Gibraltar. Journal of Geophysical Research 114, C10018. http://dx.doi.org/10.1029/2009JC005496.

Garcia-Lafuente, J., Sanchez-Roman, A., Naranjo, C., Sanchez-Garrido, J.C., 2011. The very first transformation of the Mediterranean outflow in the Strait of Gibraltar. Journal of Geophysical Research 116, C07010. http://dx.doi.org/10.1029/2011JC006967.

Garcia-Lafuente, J., Pozas, E.B., Sanchez-Garrido, J.C., Sannino, G., Sammartino, S., 2013. The interface mixing layer and the tidal dynamics at the eastern part of the Strait of Gibraltar. Journal of Marine Systems 117, 31–42. http://dx.doi.org/10.1016/j.jmarsys.2013.02.014.

Gascard, J.C., 1991. Open ocean convection and deep water formation revisited in the Mediterranean, Labrador, Greenland and Weddell Seas. In: Chu, P.C., Gascard, J.C. (Eds.), Deep Convection and Deep Water Formation in the Oceans.

Elsevier Oceanography Series, 57, Amsterdam, pp. 157–182, http://dx.doi.org/10.1016/s0422-9894(08)70066-7.
Gascard, J.C., Richez, C., 1985. Water masses and circulation in the western Alborán Sea and in the Straits of Gibraltar. Progress in Oceanography 15 (3), 157–216.
Helfrich, K.R., 1995. Time-dependent two-layer hydraulic exchange flows. Journal of Physical Oceanography 25 (3), 359–373.
Herrmann, M., Somot, S., Sevault, F., Estournel, C., Déqué, M., 2008. Modeling the deep convection in the northwestern Mediterranean Sea using an eddy-permitting and an eddy-resolving model: case study of winter 1986–1987. Journal of Geophysical Research 113, C04011. http://dx.doi.org/10.1029/2006JC003991.
Kinder, T.H., Bryden, H., 1990. Aspiration of deep waters through straits. In: Pratt, L.J. (Ed.), The Physical Oceanography of Sea Straits. Kluwer Acad., Norwell Mass., pp. 295–319, http://dx.doi.org/10.1007/978-94-009-0677-8_14.
Kinder, T.H., Parrilla, G., 1987. Yes, some of the Mediterranean outflow does come from great depth. Journal of Geophysical Research 92 (C3), 2901–2906.
Krahmann, G., 1997. Saisonale und zwischenjhrliche Variabiltim westlichen Mittelmeer-Analyse historischer Daten. Dissertation, Univ. Kiel, Kiel, Germany, 168 pp.
Lascaratos, A., Nittis, K., 1998. A high-resolution three-dimensional numerical study of intermediate water formation in the Levantine Sea. Journal of Geophysical Research 103 (C9), 18497–18511. http://dx.doi.org/10.1029/98JC01196.
Leith, C.E., 1968. Diffusion approximation for two-dimensional turbulence. Physics of Fluids 11, 671. http://dx.doi.org/10.1063/1.1691968.
Macías, D., Martin, A.P., Garcia-Lafuente, J., Garcia, C.M., Yool, A., Bruno, M., Echevarría, F., 2007. Analysis of mixing and biogeochemical effects induced by tides on the Atlantic–Mediterranean flow in the Strait of Gibraltar through a physical–biological coupled model. Progress in Oceanography 74 (2), 252–272. http://dx.doi.org/10.1016/j.ocean.2007.04.006.
Macías, D., Bruno, M., Echevarría, F., Vázquez, A., García, C.M., 2008. Meteorologically-induced mesoscale variability of the North-western Alboran Sea (southern Spain) and related biological patterns. Estuarine, Coastal and Shelf Science 78, 250–266. http://dx.doi.org/10.1016/j.ecss.2007.12.008.
Marshall, J., Schott, F., 1999. Open-ocean convection: observations, theory, and models. Reviews of Geophysics 37 (1), 1–64. http://dx.doi.org/10.1029/98RG02739.
Marshall, J., Hill, C., Perelman, L., Adcroft, A., 1997a. Hydrostatic, quasi-hydrostatic, and nonhydrostatic ocean modeling. Journal of Geophysical Research 102 (C3), 5733–5752. http://dx.doi.org/10.1029/96JC02776.
Marshall, J., Adcroft, A., Hill, C., Perelman, L., Heisey, C., 1997b. A finite-volume, incompressible Navier Stokes model for studies of the ocean on parallel computers. Journal of Geophysical Research 102, 5753–5766. http://dx.doi.org/10.1029/96JC02775.
MEDOC Group, 1969. Observations of formation of deep-water in the Mediterranean Sea. Nature 227, 1037–1040.
Mikolajewicz, U., 2011. Modeling Mediterranean Ocean climate of the last glacial maximum. Climate of the Past 7, 161–180. http://dx.doi.org/10.5194/cp-7-161-2011.
Naranjo, C., Garcia-Lafuente, J., Sanchez-Garrido, J.C., Sanchez-Roman, A., Delgado Cabello, J., 2012. The western Alborán gyre helps ventilate the western Mediterranean deep water through Gibraltar. Deep Sea Research Part I: Oceanographic Research Papers 63, 157–163. http://dx.doi.org/10.1016/j.dsr.2011.10.003.
Oddo, P., Adani, M., Pinardi, N., Fratianni, C., Tonani, M., Pettenuzzo, D., 2009. A nested Atlantic–Mediterranean Sea general circulation model for operational forecasting. Ocean Science Discussions 5 (461–473), 2009. http://dx.doi.org/10.5194/os-5-461-2009.
Pacanowski, R.C., Philander, S.G.H., 1981. Parameterization of vertical mixing in numerical models of tropical oceans. Journal of Physical Oceanography 11 (11), 1443–1451.
Pinardi, N., Zavatarelli, M., Adani, M., Coppini, G., Fratianni, C., Oddo, P., Bonaduce, A., 2013. Mediterranean Sea large-scale low-frequency ocean variability and water mass formation rates from 1987 to 2007: a retrospective analysis. Progress in Oceanography. http://dx.doi.org/10.1016/j.pocean.2013.11.003 (in press).
Sammartino, S., Garcia-Lafuente, J., Sanchez-Garrido, J.C., De los Santos, F.J., ÁlvarezFanjul, E., Naranjo, C., Bruno, M., Calero, C., 2014. A numerical model analysis of the tidal flows in the Bay of Algeciras, Strait of Gibraltar. Continental Shelf Research 72, 34–46. http://dx.doi.org/10.1016/j.csr.2013.11.002.
Sanchez-Garrido, J.C., Sannino, G., Liberti, L., Garcia-Lafuente, J., Pratt, L., 2011. Numerical modeling of three-dimensional stratified tidal flow over Camarinal Sill, Strait of Gibraltar. Journal of Geophysical Research 116, C12026. http://dx.doi.org/10.1029/2011JC007093.
Sanchez-Garrido, J.C., Garcia-Lafuente, J., Álvarez-Fanjul, E., Sotillo, M., de-los-Santos, F.J., 2013. What does cause the collapse of the Western Alborán Gyre? Results of an operational ocean model. Progress in Oceanography 116, 142–153. http://dx.doi.org/10.1016/j.pocean.2013.07.002.
Sanchez-Román, A., Sannino, G., Garcia-Lafuente, J., Carillo, A., Criado-Aldeanueva, F., 2009. Transport estimates at the western section of the Strait of Gibraltar: a combined experimental and numerical modeling study. Journal of Geophysical Research 114, C06002. http://dx.doi.org/10.1029/2008JC005023.
Sannino, G., Bargagli, A., Artale, V., 2004. Numerical modeling of the semidiurnal tidal exchange through the Strait of Gibraltar. Journal of Geophysical Research 109, C050115. http://dx.doi.org/10.1029/2003JC002057.
Sannino, G., Carillo, A., Artale, V., 2007. Three-layer view of transports and hydraulics in the Strait of Gibraltar: a three-dimensional model study. Journal of Geophysical Research 112, C03010. http://dx.doi.org/10.1029/2006JC003717.
Sannino, G., Sanchez Garrido, J.C., Liberti, L., Pratt, L., 2014. Exchange flow through the Strait of Gibraltar as simulated by a σ-coordinate hydrostatic model and a z-coordinate nonhydrostatic model. In: Borzelli, G.L.E., Gačić, M., Lionello, P., Malanotte-Rizzoli, P. (Eds.), The Mediterranean Sea: Temporal Variability and Spatial Patterns. John Wiley & Sons Inc., Oxford. http://dx.doi.org/10.1002/9781118847572.ch3.
Schott, F., Visbeck, M., Send, U., 1994. Open ocean deep convection, Mediterranean and Greenland Seas. In: Malanotte-Rizzoli, P., Robinson, A.R. (Eds.), Ocean Processes on Climate Dynamics: Global and Mediterranean Examples. Kluwer Acad., Norwell, Mass., pp. 203–225.
Schott, F., Visbeck, M., Send, U., Fischer, J., Stramma, L., Desaubies, Y., 1996. Observations of deep convection in the Gulf of Lions, northern Mediterranean, during the winter of 1991/92. Journal of Physical Oceanography 26 (4), 505–524. http://dx.doi.org/10.1175/1520-0485(1996) 026<0505:OODCIT>2.0.CO;2.
Schroeder, K., Ribotti, A., Borghini, M., Sorgente, R., Perilli, A., Gasparini, G.P., 2008. An extensive western Mediterranean deep water renewal between 2004 and 2006. Geophysical Research Letters 35, L18605. http://dx.doi.org/10.1029/2008GL035146.
Send, U., Schott, F., Gaillard, F., Desaubies, Y., 1995. Observation of a deep convection regime with acoustic tomography. Journal of Geophysical Research 100 (C4), 6927–6941. http://dx.doi.org/10.1029/94JC03311.
Smith, R.O., Bryden, H.L., Stansfield, K., 2008. Observations of new western Mediterranean deep water formation using Argo floats 2004–2006. Ocean Science 4 (2), 133–149.
Stommel, H., Bryden, H., Mangelsdorf, P., 1973. Does some of the Mediterranean outflow come from great depth? Pure and Applied Geophysics 105 (1), 879–889.
Tziperman, E., Speer, K., 1994. A study of water mass transformation in the Mediterranean Sea: analysis of climatological data and a simple three-box model. Dynamics of Atmospheres and Oceans 21, 53–82. http://dx.doi.org/10.1016/0377-0265(94)90004-3.
Vargas, J.M., Garcia-Lafuente, J., Candela, J., Sanchez, A.J., 2006. Fortnightly and monthly variability of the exchange through the Strait of Gibraltar. Progress in Oceanography 70 (2), 466–485. http://dx.doi.org/10.1016/j.pocean.2006.07.001.
Vázquez, A., Bruno, M., Izquierdo, A., Macías, D., Ruiz-Cañavate, A., 2008. Meteorologically forced subinertial flows and internal wave generation at the main sill of the Strait of Gibraltar. Deep Sea Research Part I: Oceanographic Research Papers 55 (10), 1277–1283. http://dx.doi.org/10.1016/j.dsr.2008.05.008.
Vázquez, A., Flecha, S., Bruno, M., Macías, D., Navarro, G., 2009. Internal waves and short-scale distribution patterns of chlorophyll in the Strait of Gibraltar and Alborán Sea. Geophysical Research Letters 36 (23), L23601. http://dx.doi.org/10.1029/2009GL040959.
Wang, D.P., 1993. The Strait of Gibraltar Model: internal tide, diurnal inequality and fortnightly modulation. Deep Sea Research Part I: Oceanographic Research Papers 40 (6), 1187–1203. http://dx.doi.org/10.1016/0967-0637(93)90133-N.
Wesson, J.C., Gregg, M.C., 1994. Mixing at Camarinal sill in the Strait of Gibraltar. Journal of Geophysical Research: Oceans 99 (5), 9847–9878. http://dx.doi.org/10.1029/94JC00256 (1978–2012).
Whitehead Jr., J.A., 1985. A laboratory study of gyres and uplift near the Strait of Gibraltar. Journal of Geophysical Research 90 (C4), 7045–7060. http://dx.doi.org/10.1029/JC090iC04p07045.